Short-Term and Long-Term Surface Soil Moisture Memory Time Scales Are Spatially Anticorrelated at Global Scales

KAIGHIN A. MCCOLL

Harvard University, Cambridge, Massachusetts

QING HE AND HUI LU

Ministry of Education Key Laboratory for Earth System Modeling, and Department of Earth System Science, Tsinghua University, Beijing, China

DARA ENTEKHABI

Massachusetts Institute of Technology, Cambridge, Massachusetts

(Manuscript received 10 July 2018, in final form 19 March 2019)

ABSTRACT

Land–atmosphere feedbacks occurring on daily to weekly time scales can magnify the intensity and duration of extreme weather events, such as droughts, heat waves, and convective storms. For such feedbacks to occur, the coupled land–atmosphere system must exhibit sufficient memory of soil moisture anomalies associated with the extreme event. The soil moisture autocorrelation *e*-folding time scale has been used previously to estimate soil moisture memory. However, the theoretical basis for this metric (i.e., that the land water budget is reasonably approximated by a red noise process) does not apply at finer spatial and temporal resolutions relevant to modern satellite observations and models. In this study, two memory time scale metrics are introduced that are relevant to modern satellite observations and models: the "long-term memory" τ_L and the "short-term memory" τ_S. Short- and long-term surface soil moisture (SSM) memory time scales are spatially anticorrelated at global scales in both a model and satellite observations, suggesting hot spots of land–atmosphere coupling will be located in different regions, depending on the time scale of the feedback. Furthermore, the spatial anticorrelation between τ_S and τ_L demonstrates the importance of characterizing these memory time scales separately, rather than mixing them as in previous studies.

1. Introduction

Land–atmosphere feedbacks occurring on daily to weekly time scales play a crucial role in the timing and severity of extreme events, including droughts, heat waves (Miralles et al. 2014; Roundy et al. 2014, 2013), and convective storms (Findell and Eltahir 2003a,b; Gentine et al. 2013; Guillod et al. 2015). For example, a precipitation event can lead to increased soil moisture, which can lead to increased evapotranspiration and, ultimately, the development of clouds and further precipitation (Seneviratne et al. 2010). Properly representing these feedbacks in models is a long-standing challenge since they are emergent features of coupled physical processes (including evapotranspiration and the surface energy balance, boundary layer growth and decay, and deep convection) that are parameterized, rather than resolved, by most models. The absence of such feedbacks in models compromises their skill in predicting extreme events. Their absence may also contribute to model deficiencies at the land surface: for example, the observed rapid-onset warm bias in surface temperatures that appears in most weather and climate models over midlatitude inland continental regions (Klein et al. 2006; Ma et al. 2018, 2014; Morcrette et al. 2018). As such, characterizing land–atmosphere feedbacks with observations is a key priority for addressing model deficiencies at the land–atmosphere interface (Santanello et al. 2018).

The coupled system must exhibit sufficient "memory" for these feedbacks to occur. For example, if additional

Denotes content that is immediately available upon publication as open access.

Kaighin A. McColl and Qing He contributed equally.

Corresponding author: Kaighin A. McColl, kmccoll@seas.harvard.edu

DOI: 10.1175/JHM-D-18-0141.1

moisture from a precipitation event rapidly drains out of a soil volume into deeper reservoirs, then there is no time for the moisture to be evaporated or transpired into the atmosphere or influence the surface energy balance, and the feedback loop cannot occur. More specifically, the memory of the soil moisture storage is defined as the time taken to dissipate an anomaly, where an anomaly is typically defined as a deviation from some climatological reference value. There are substantial differences in estimated soil moisture memory across models (Koster and Suarez 2001; Seneviratne et al. 2006; Seneviratne and Koster 2012), suggesting model-based estimates are highly uncertain.

Most previous studies estimate soil moisture memory using a metric based on the autocorrelation of the soil moisture time series. Delworth and Manabe (1989, 1988) first proposed this metric by noting that, at large temporal and spatial scales, soil moisture time series can be reasonably represented as a red noise process. To justify this model, they first noted that the vertically integrated land water anomaly budget for a planar homogeneous soil volume is

$$\Delta z \frac{d\theta'(t)}{dt} = P'(t) - L'(t) = P'(t) - \mathrm{ET}'(t) - Q'(t), \quad (1)$$

where Δz is the depth of the hydrologically active soil control volume, θ is the volumetric soil moisture, P is precipitation, ET is evapotranspiration, Q is drainage and runoff, $L = \mathrm{ET} + Q$ is the "loss function," and primed quantities are anomalies [e.g., $\theta'(t) = \theta(t) - \overline{\theta}$, where $\overline{\theta}$ is the time average soil moisture; and similarly for P', ET′, Q', and L']. Assuming that 1) P' can be represented as a white noise process; 2) ET′ can be approximated as a linear function of soil moisture; and 3) Q' can be neglected when considering the entire soil column over large scales relevant to climate models, the land water anomaly budget can be rewritten as

$$\frac{d\theta(t)}{dt} = -\frac{\theta(t) - \overline{\theta}}{T} + \varepsilon(t), \quad (2)$$

where T is a fixed parameter that is a function of Δz and the sensitivity of ET′ to soil moisture, and $\varepsilon(t)$ is an independent and identically distributed random variable with a mean of zero. This expression is the definition of a red noise process. The e-folding autocorrelation time scale of a red noise process is simply T, which Delworth and Manabe (1989, 1988) first proposed as a useful time scale of soil moisture memory when applied to monthly model outputs and has since been widely adopted (e.g., Dirmeyer et al. 2016; Dirmeyer and Norton 2018; Entin et al. 2000; Vinnikov and Yeserkepova 1991). Since then, other memory metrics based on the autocorrelation function have also been employed, including the integral time scale (e.g., Ghannam et al. 2016; Katul et al. 2007), the autocorrelation for a fixed time lag (e.g., Koster and Suarez 2001; Seneviratne et al. 2006), and the soil moisture variance spectrum (e.g., Katul et al. 2007; Nakai et al. 2014). All of these measures of soil moisture memory relate back to a model of soil moisture as a stochastic, red noise process [Eq. (2)].

However, this model was designed for coarse temporal and spatial scales and breaks down at finer resolutions relevant to newer models and satellite observations. As an illustration of this problem (which focuses on fine temporal rather than spatial scales), we use synthetic soil moisture "observations"—generated from a simple water balance model with prescribed loss function and forced with stochastic precipitation [described in appendix B, and similar to, e.g., Laio et al. (2001) and Feng et al. (2014)]—to examine the impact of temporal averaging on estimates of memory time scales. The prescribed loss function (Figs. 1a–d, solid black line) has a standard form, comprising a regime in which drainage dominates for high soil saturation $s = \theta/n$ (n is soil porosity) where the loss function follows a power law with soil moisture; a stage-I ET regime for intermediate values of s, in which the loss function is invariant with soil moisture; and a stage-II ET regime for low s, in which the loss function is linear with soil moisture. The soil moisture outputs are averaged in blocks of length Δt days. Precipitation is similarly accumulated. Losses at temporal resolution Δt are then estimated by subtracting changes in averaged soil moisture (at time scale Δt) from precipitation (accumulated at time scale Δt) and compared with the "true" instantaneous loss function used to generate the synthetic soil moisture. For $\Delta t = 30$ days (Figs. 1b,d), the estimated loss function is substantially different compared to the instantaneous loss function for all soil moisture values, caused by averaging to coarser time scales. It is represented reasonably by a linear function (gray dashed line) with substantial additive random noise; in other words, it can be reasonably modeled stochastically—as a red noise process [Eq. (2)]—at a temporal resolution of $\Delta t = 30$. This is similar to the formulation for rapid surface runoff used in a simple water balance model proposed in previous studies (Koster 2015; Koster and Milly 1997; Koster and Mahanama 2012).

In contrast, for $\Delta t = 3$ days, the estimated loss function fits the instantaneous loss function very well for drier soil moisture values. This is because more variability is resolved by the soil moisture time series at a temporal scale of $\Delta t = 3$ days (Figs. 1a,c) compared to $\Delta t = 30$ days. Therefore, a deterministic loss model

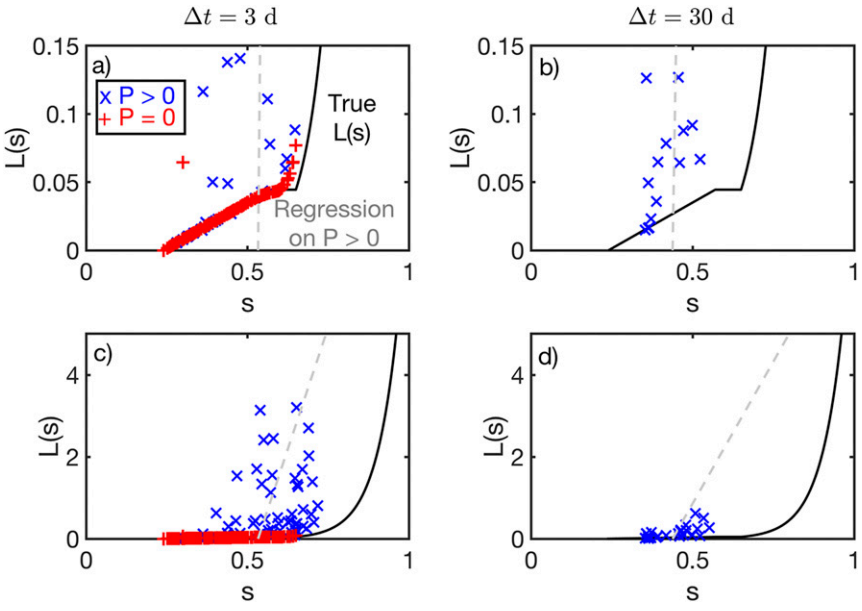

FIG. 1. (a) Instantaneous loss function $L(s)$ estimated from synthetic soil saturation observations $s = \theta/n$, where n is soil porosity. The synthetic soil moisture time series were generated using a prescribed loss function (black solid line). After averaging the synthetic soil moisture to a temporal resolution $\Delta t = 3$ days, the estimated losses (crosses) are partitioned based on the occurrence of precipitation. For $P = 0$, the estimated losses (red crosses) reasonably match the true loss $L(s)$, i.e., the loss function is "resolved" by the observations at $\Delta t = 3$ when $P = 0$. The long-term memory τ_L is inversely proportional to the slope of the loss function in this resolved range. For $P > 0$, the estimated losses (blue crosses) deviate substantially from $L(s)$, i.e., the loss function is not resolved by the observations at $\Delta t = 3$ when $P > 0$. The short-term memory τ_S is inversely proportional to the slope of the (gray dashed) line fit to the estimated losses for which $P > 0$ (blue crosses). (b) As in (a), but with $\Delta t = 30$ days. (c) As in (a), but different y-axis limits. (d) As in (b), but different y-axis limits.

appears most appropriate for dry conditions. However, at higher soil moisture values, the estimated loss function differs substantially compared to the instantaneous loss function. These losses are larger and occur more rapidly compared to those at lower soil moisture values, and are not resolved by the soil moisture time series even at $\Delta t = 3$ days. The scatter suggests a stochastic loss model (perhaps similar to the red noise model) is more appropriate under wet conditions. Overall, a model of the loss function that is purely deterministic or purely stochastic (like the red noise model) will be inadequate at this temporal resolution.

This is a common problem across disciplines in climate modeling: a parameterization designed for a coarse temporal or spatial scale may not translate well to finer temporal or spatial scales that become feasible to model or observe as computational resources and satellite observation resolutions increase with time [e.g., Wyngaard (2004) describes a conceptually analogous modeling problem in atmospheric science]. Why does this occur? In the original work on soil moisture memory by Delworth and Manabe (1989, 1988), soil moisture drydowns—common features of any soil moisture time series, in which the soil moisture decays quasi-exponentially following a precipitation event (Fig. 2a)—typically occurred on time scales much shorter than the model's (coarse) output frequency; that is, the drydowns were not resolved in the model output (Fig. 2c). This justified their treatment as stochastic fluctuations around a more slowly varying mean soil moisture state; that is, the application of the red noise model [Eq. (2)]. However, as model resolutions have increased and satellite observations have become available, drydowns have become at least partially resolved in both standard model outputs and in global observations (Fig. 2b). To borrow terminology from the atmospheric boundary layer community, our models and satellite observations of soil moisture are in the resolution "gray zone" (e.g., Honnert 2016), which we define here as time scales of days to weeks, and spatial scales from $O(1)$ to $O(10)$ km. Treating soil moisture drydowns as stochastic fluctuations is no longer justified; yet, since they are not fully resolved

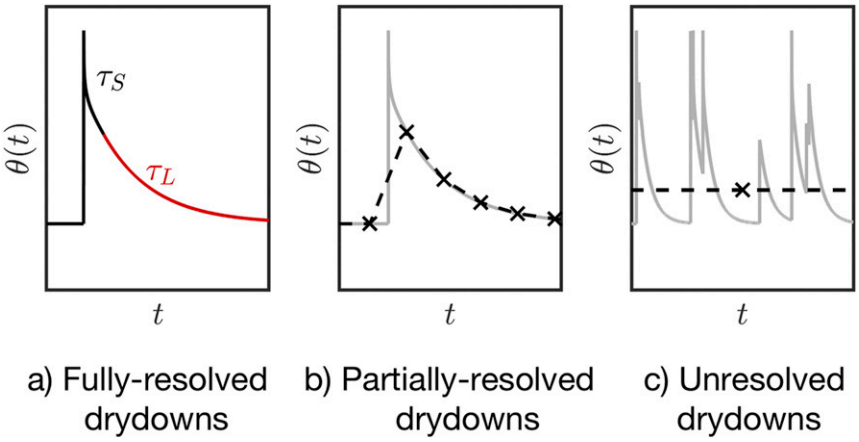

FIG. 2. (a) Soil moisture drydowns can be approximated with two decay time scales: a rapid drainage time scale (the short-term memory τ_S), and a slower ET time scale (the long-term memory τ_L). For sufficiently high sampling frequencies, both time scales can be estimated from the soil moisture time series. (b) For sampling frequencies typical of modern satellite observations, only the later stages of the drydown (governed by τ_L) are resolved. (c) In older models, at temporal scales of weeks to months, most drydowns are not resolved.

(and will not be in global satellite observations for the foreseeable future), they can be treated as, at best, only partially deterministic.

In this study, we introduce a hybrid model of soil moisture memory that can be applied in the gray zone. Our model builds on the red noise model of soil moisture memory [Eq. (2)]. It replaces the one parameter of the red noise model (T, the e-folding autocorrelation time scale) with two parameters: the ''short-term memory'' τ_S and the ''long-term memory'' τ_L. The details of the hybrid model are presented in section 2. Quantities related to τ_S and τ_L have been estimated in recent studies (McColl et al. 2017a,b; Shellito et al. 2018, 2016). However, while these quantities have been analyzed individually, they have not been analyzed jointly. For example, the relation between short-term and long-term memory is unclear: do regions with significant short-term memory also tend to have significant long-term memory? Furthermore, most previous studies have focused on satellite observations. It is unclear how models perform in this respect, and the extent of disagreement with satellite observations. In response to these knowledge gaps, in this paper, we perform a joint analysis of both memory time scales, using both satellite observations and a land surface model. The three main contributions of this study are in 1) reconceptualizing soil moisture memory, moving away from a stochastic model that fails at fine spatial and temporal scales, to a hybrid model that is more appropriate to the gray zone, and breaks memory down into short-term and long-term components; 2) comparing estimates of short-term and long-term memory and analyzing their relation globally; and 3) contrasting with estimates from a global land surface model. From this joint analysis, we find that 1) the model examined in this study tends to overestimate long-term memory and underestimate short-term memory of surface soil moisture relative to satellite observations and 2) regions with relatively long short-term memory tend to have relatively short long-term memory, and vice versa, in both the model and satellite observations.

This paper is structured as follows. In section 2, we introduce the hybrid soil moisture memory model, describe procedures for robustly estimating τ_S and τ_L from model outputs and satellite observations, and describe the datasets used in this study. In section 3, we present and discuss the results of our analyses: comparing global estimates of τ_S and τ_L from a model and satellite observations and analyzing their correlation in space. Conclusions are summarized in section 4.

2. Methods and data

In this section, we present the hybrid soil moisture memory model and procedures for estimating τ_S and τ_L from soil moisture time series and describe the soil moisture and precipitation datasets used in this study.

Building on the stochastic red noise model of soil moisture memory, we propose a hybrid stochastic–deterministic model, designed for the gray zone. The hybrid model includes a deterministic component under dry conditions, and a stochastic component under wet conditions. To separate the deterministic component

from the stochastic component, we condition on the occurrence of precipitation. Losses estimated in time blocks (i.e., an interval $[t - \Delta t, t]$, where t is time and Δt is the temporal resolution of model outputs or satellite observations) where precipitation occurred are assumed to be generated by the stochastic component; losses estimated in time blocks where precipitation did not occur are assumed to be generated by the deterministic component. This partitioning separates the two components well in our simulation (Figs. 1a–d). The model can be written as

$$\frac{d\theta(t)}{dt} = \begin{cases} -\dfrac{\theta(t) - \theta_w}{\tau_L}, & \text{if} \quad P = 0 \text{ in the interval } [t - \Delta t, t], \\ -\dfrac{\theta(t) - \overline{\theta}}{\tau_S} + \varepsilon(t), & \text{if} \quad P > 0 \text{ in the interval } [t - \Delta t, t], \end{cases} \tag{3}$$

where θ_w is a minimum soil moisture value, and $\overline{\theta}$ and ε have the same definitions as in Eq. (2). Here, τ_L is a memory time scale controlled by stage-II ET that is resolved by the observations; we call this the long-term memory. In contrast, τ_S is a memory time scale governed by a combination of unresolved processes, particularly, but not exclusively, drainage (the vertical flux of moisture out of the bottom of the soil moisture control volume, deeper into the unsaturated zone); we call this the short-term memory. Note that this model of memory essentially reduces to the original red noise model when applied to the $\Delta t = 30$ days observations since $P > 0$ for nearly all time blocks; in this case, τ_S and T are equivalent. However, fitting a red noise model to the $\Delta t = 3$ days observations would mix the quite distinct time scales τ_L and τ_S, resulting in a memory time scale estimate that is not representative of either the resolved stage-II ET regime, nor the unresolved regime.

The hybrid model [Eq. (3)] requires information on precipitation occurrence (a binary variable). However, remotely sensed precipitation observations likely have significantly larger errors compared to satellite soil moisture observations. Therefore, to avoid introducing a separate precipitation time series into the analysis, we use positive increments in the surface soil moisture time series as a proxy for precipitation occurrence. At small scales (from point scales to field scales), positive increments in surface soil moisture can be caused by a variety of mechanisms, including run-on, capillary rise, irrigation, and precipitation events. At larger scales, however, almost all positive increments in the surface soil moisture time series are caused by precipitation events. As a simplification, we assume that all positive increments in the surface soil moisture time series are caused by precipitation events for models or observations of surface soil moisture at large scales, while acknowledging that this is an approximation that may not be strictly true in all cases (McColl et al. 2017a).

a. *Estimation of long-term memory* τ_L

We first explain the estimation of τ_L, which follows the same method as McColl et al. (2017b), and is briefly summarized. Drydowns are identified in the soil moisture time series as periods in which the change in soil moisture is consistently negative. To mitigate against noise in the soil moisture time series, the length of the drydown and the size of increments must be greater than prescribed thresholds (in this study, the drydown must be based on at least three observations, and the increment must be at least 10% of the observed range of the soil moisture time series). The governing equation for each identified drydown corresponds to the case where $P = 0$ in the hybrid model [Eq. (3)]. This equation can be solved to give the relation:

$$\theta(t) = \Delta\theta \exp\left(-\frac{t - \Delta t_P}{\tau_L}\right) + \theta_w. \tag{4}$$

This function is fit to each observed drydown using nonlinear least squares fitting, to estimate τ_L (McColl et al. 2017b; Rondinelli et al. 2015; Shellito et al. 2018, 2016). Here, $\Delta\theta$ is the drydown amplitude, θ_w is a minimum soil moisture value for the given location, and $t = \Delta t_P$ at the start of an individual drydown. The parameter θ_w is constrained to be lower than the lowest soil moisture value observed during the drydown. In cases where the fitted curve had a coefficient of determination R^2 less than 0.7, the drydown was discarded from the analysis. If fewer than three drydowns were identified in a given location, the grid cell was masked out.

This approach assumes that the resolved component of the drydown (for $\Delta t = 3$ days) lies entirely within the stage-II ET regime; while this is not strictly true in all cases, McColl et al. (2017b) showed that it is a reasonable assumption based on model experiments. A desirable property of this estimation procedure is that it automatically restricts the analysis to regions where ET is sensitive to soil moisture, since these are the only

regions in which drydowns [of the form given in Eq. (4)] will be visible in the soil moisture time series. In regions where ET is relatively insensitive to soil moisture, soil moisture–precipitation feedbacks cannot occur.

An alternative approach to estimating τ_L would be to fit a linear relation between $\theta(t)$ and $d\theta(t)/dt$, restricted to cases in which $P = 0$. However, in this case, comparable errors are present in both the independent and dependent variables [$\theta(t)$ and $d\theta(t)/dt$, respectively], in violation of standard ordinary least squares assumptions. Instead, more sophisticated regression procedures could be used (e.g., errors-in-variables approaches), but these methods require information on the error structures of $\theta(t)$ and $d\theta(t)/dt$. Instead, by regressing $\theta(t)$ on the error-free independent variable t, rather than regressing $d\theta(t)/dt$ on $\theta(t)$, we avoid this problem, but at the cost of a more complicated nonlinear fitting procedure.

b. Estimation of short-term memory τ_S

In this section, we describe the estimation procedure for τ_S. Rather than performing a linear regression in [$\theta(t)$, $d\theta(t)/dt$] space, restricted to cases where $P > 0$, we adopt a similar approach to the previous section, in which a nonlinear drydown model is fit in [t, $\theta(t)$] space. However, since the beginning of the drydown is typically not resolved by the observations for $\Delta t = 3$ days (Fig. 2b), we require additional assumptions compared to the procedure for estimating τ_L. The three additional assumptions relate to the unobserved initial condition for the drydown:

R1: The precipitation event that precedes the drydown, which is not resolved by the soil moisture time series, is assumed to occur randomly between the two soil moisture observations comprising the positive increment. That is, for a positive increment $\Delta\theta_+(t) = \theta(t) - \theta(t - \Delta t) > 0$, the timing of the precipitation event causing the positive increment is assumed to be uniformly distributed on the interval $[t - \Delta t, t]$. This assumption is reasonable given the sampling frequency of the soil moisture observations is uncorrelated with precipitation.

R2: The soil moisture value at the unobserved start of the drydown is, on average, assumed to be $\overline{\theta(t - \Delta t)} + \alpha/\Delta z$, where α is mean event precipitation. Implicitly, this assumes that, at large scales, positive increments in the soil moisture time series are always caused by precipitation. This assumption will be violated in some regions where irrigation, capillary rise and/or run-on are substantial; but at large scales, relatively few grid points are expected to be influenced by these effects substantially.

R3: The mean soil moisture $\overline{\theta}$ is a reasonable approximation of the mean soil moisture value immediately prior to a precipitation event $\overline{\theta(t - \Delta t)}$. This assumption was tested in a suite of synthetic experiments (appendix B) and was found to be reasonable (not shown).

Combining assumptions R1–R3 with the hybrid model [Eq. (3), focusing on the $P(t) > 0$ case] gives an explicit expression for the short-term memory:

$$\tau_S = -\frac{\frac{\Delta t}{2}}{\log\left(\frac{\Delta z \overline{\Delta\theta_+}}{\alpha}\right)} = -\frac{\frac{\Delta t}{2}}{\log(F_P)}, \tag{5}$$

where F_P is the "stored precipitation fraction" introduced in McColl et al. (2017a). A full derivation of this relation is provided in appendix A.

The procedures described here for estimating τ_S and τ_L are not the only possible approaches. Several techniques exist for directly estimating the loss function $L(s)$ using soil moisture observations. Since τ_L and τ_S are inverse slopes of the loss function in the stage-II ET regime, and a combination of the unresolved stage-I ET and drainage regimes, respectively, these techniques provide implicit estimates of τ_L and τ_S. Salvucci (2001) showed that the loss function, evaluated at a particular soil moisture value, is equivalent to the mean precipitation conditioned on that soil moisture value. Observed precipitation time series can, therefore, be combined with observed soil moisture time series to estimate the loss function (Saleem and Salvucci 2002; Salvucci 2001; Tuttle and Salvucci 2014). Koster et al. (2017) proposed an alternative approach in which the loss function is calibrated piecewise based on a water balance forced with observed precipitation and soil moisture time series. In contrast, Akbar et al. (2018a) estimated the loss function based on negative increments in the soil moisture time series, without using precipitation observations. The techniques we propose for estimating τ_S and τ_L require observed soil moisture time series, and mean event precipitation (but not precipitation time series). Our approach lies somewhere between those of Salvucci (2001) and Koster et al. (2017)—which require observed precipitation time series that might be more error-prone than mean event precipitation, but make fewer assumptions about the shape of the loss function—and Akbar et al. (2018a) which requires no precipitation observations, but may be less accurate in estimating τ_S.

A major advantage of our memory estimates is that they are not dependent on a reference value. Autocorrelation-based metrics are defined with respect to a reference state, which can be an annual mean, time-varying trend, or other value. For example, previous studies that estimated memory based on autocorrelation-based metrics often limited their analyses to the Northern Hemisphere summer [June–August (JJA)], using JJA mean soil moisture as the reference value (e.g., Dirmeyer et al. 2016; Koster and Suarez 2001; Seneviratne et al. 2006). Unfortunately, this severely complicates comparisons with, for example, regions in the Southern Hemisphere (for which JJA is winter). The seasonal cycle also leaks into the estimated memory time scale, often increasing it substantially (Koster and Suarez 2001; Seneviratne and Koster 2012). In contrast, since our estimates of τ_S and τ_L are based on localized features of the soil moisture time series (positive increments for τ_S, and drydowns for τ_L) and are not dependent on fixed reference values, we are able to make concurrent, global estimates of surface soil moisture (SSM) memory time scales using a single estimation procedure. Both short- and long-term memory estimates are also largely insensitive to the seasonal cycle (appendix B, Fig. B1).

A second major advantage of our approach is that it does not mix two different time scales. Autocorrelation-based metrics assume a red noise model [i.e., a noisy, linear relation between $L(s)$ and s]; but fitting such a model to, for instance, the example case in Fig. 1a, would result in an estimated time scale (proportional to the inverse slope) that is a mixture of τ_L and τ_S. This is particularly significant since, as we will show, τ_L and τ_S are spatially anticorrelated at global scales. Therefore, an autocorrelation-based memory time scale is often a mixture of relatively high τ_L and relatively low τ_S, or vice versa, resulting in a spatial distribution that is substantially different to those of both τ_L and τ_S. Spatial gradients apparent in τ_L and τ_S are smoothed out by this mixing, resulting in a more uniform spatial field for standard autocorrelation-based time scales.

c. SMAP soil moisture data

We use surface soil moisture observations from NASA's Soil Moisture Active Passive (SMAP) mission. Launched in January 2015, SMAP measures surface soil moisture (i.e., moisture in the top ~5 cm of soil) globally using a passive L-band radiometer (Entekhabi et al. 2010) at 36 km spatial resolution. We use two years of morning overpass, version 4 SMAP passive soil moisture retrievals, spanning 1 April 2015–31 March 2017 (O'Neill et al. 2018). We use morning observations because the assumption of equal surface and air temperatures that is made in the SMAP retrieval algorithm is more likely to be satisfied early in the morning. This appears to be a sufficiently large sample size to characterize annual average properties relevant to soil moisture memory.

Validation studies demonstrate that SMAP is meeting its performance target (Chan et al. 2016; Colliander et al. 2017), and has the highest global accuracy (measured by its correlation coefficient) when compared with two other soil moisture satellites (Chen et al. 2018). The data were filtered to limit the effects of potential error sources—such as radio frequency interference (RFI), the presence of small water bodies, dense vegetation (tropical and boreal forests where the estimated vegetation water content exceeds 5 kg m^{-2}), and frozen landscapes—as described in a previous study (McColl et al. 2017b). While SMAP's sampling frequency is nominally once every 3 days, it deviates from this in some locations due to the satellite's orbital geometry. Filtering also reduces the number of satellite observations available in some locations, which reduces the "effective sampling frequency," that is, the ratio of the total number of observations available to the number of days in the study period. In most regions, there are at least 100 observations available after filtering (see Fig. S9 of McColl et al. 2017b). Estimates of τ_S and τ_L are both partially dependent on the sampling frequency of the observations (McColl et al. 2017a,b). Spatially coherent patterns in sampling frequency of the observations can, therefore, lead to spatially coherent patterns in maps of τ_S and τ_L, which can be misinterpreted as physical signals rather than observational artifacts. To mitigate the effects of this problem, we undersample the SMAP observations (i.e., discard observations) in regions where the sampling frequency is greater than once every 3 days to obtain an effective sampling frequency close to the nominal SMAP value.

SMAP (like all soil moisture satellites at time of writing) measures SSM rather than root-zone soil moisture (RZSM), which is often the more important control on processes such as ET. However, in many cases, SSM is well correlated with RZSM (Akbar et al. 2018b; Ford et al. 2014), meaning SSM can be regarded as a reliable proxy of RZSM under many (although not all) conditions.

d. GPM precipitation data

Precipitation observations are obtained from the NASA Global Precipitation Mission (GPM) at 0.1° resolution, for the same 2-yr period as the SMAP observations. Due to its orbit, GPM provides observations at latitudes between

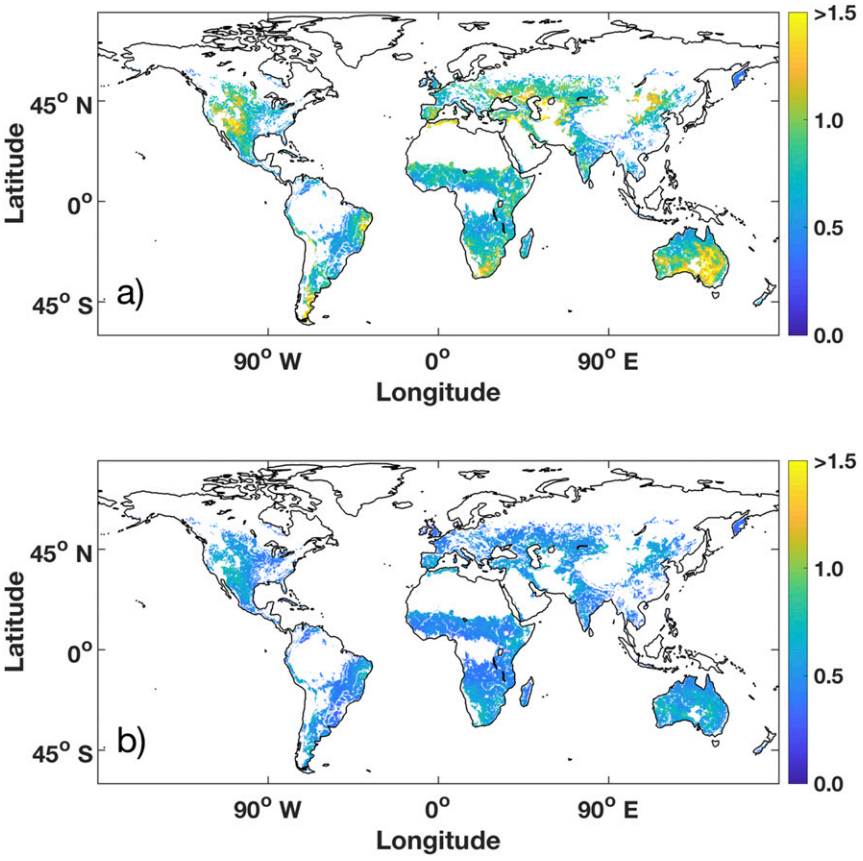

FIG. 3. Global map of short-term memory τ_S (days) estimated from (a) satellite observations and (b) model SSM.

60°S and 60°N. The specific products used are the half-hourly Final-Run (Huffman 2017) and Late-Run Integrated Multi-Satellite Retrievals for GPM (IMERG) products. The observations are regridded to SMAP's EASE 2.0 grid and filtered to exclude regions in which total precipitation is zero.

e. *GEOS-5 Catchment land surface model*

In addition to estimating τ_S and τ_L from observations, we also estimate these parameters using an offline land surface model. We use the ''Nature Run version 4'' simulation performed by Reichle et al. (2017a) using the Goddard Earth Observing System Model, version 5 (GEOS-5), Catchment land surface model, which has a native resolution of 9 km (Ducharne et al. 2000; Koster et al. 2000). An advantage of this model is that it has an explicit top 5 cm surface soil moisture layer, which matches the nominal SMAP sensing depth. Full details of the model run can be found in Reichle et al. (2017a).

We use both Nature Run surface soil moisture (top 0–5 cm) and root-zone soil moisture (top 0–100 cm) to estimate both τ_S and τ_L globally. The SMAP measurement depth is nominally top 0–5 cm and is validated against in situ observations at this depth. However, the actual SMAP measurement depth varies with soil moisture content and other variables. Therefore, to allow a fair comparison with the model, we compare SMAP observations to both SSM and RZSM model outputs.

The data are filtered consistent with the SMAP observations. Furthermore, to isolate the impact of soil moisture observations on our comparison between models and observations, we use GPM precipitation to estimate τ_S from the Nature Run using Eq. (5) rather than the precipitation used as forcing in the Nature Run. If we did not do this, differences between model and satellite estimates of τ_S could, in theory, be due to differences in precipitation forcing. Reichle et al. (2017b) compared the gauge-corrected precipitation forcing used in the Nature Run to a combination of GPM and Tropical Rainfall Measuring Mission (TRMM) precipitation observations. They found that, while there were important differences in the diurnal

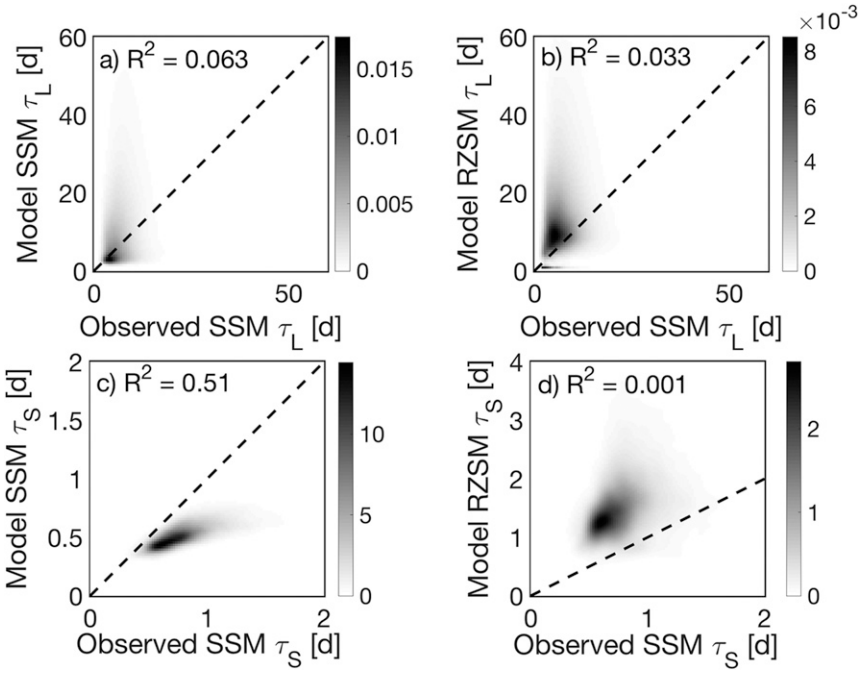

FIG. 4. Comparisons of modeled and satellite-observed τ_S and median τ_L. Shaded areas are estimated joint empirical distribution functions of the variables listed on the x and y axes. Dashed lines are 1:1 lines.

cycle phase between the products, the diurnal amplitudes were largely similar, albeit with exceptions in areas with few gauge observations. Since we only require an estimate of the event-mean precipitation rate, the GPM and Nature Run precipitation forcing are comparable for our purposes.

3. Results and discussion

In this section, we present estimates of τ_S and τ_L from SMAP satellite observations and compare with those obtained using model SSM and RZSM; and assess the spatial relation between τ_S and τ_L in the model and satellite observations.

a. Comparison between model and satellite observations

The land surface model systematically underestimates SSM τ_S in most parts of the world relative to satellite observations (Fig. 3). However, the model is more successful in capturing spatial patterns in SSM τ_S: after a linear rescaling to remove additive and multiplicative biases, it explains 51% of the observed spatial variance (Fig. 4c). In particular, there is a bimodal spatial structure over North America, with larger values in the west compared to the east. This pattern is similar to that observed in McColl et al. (2017a), who used SMAP observations to plot F_P [recall that τ_S is a monotonic increasing function of F_P; see Eq. (5)]. It is particularly noteworthy because of its relation to the work of Tuttle and Salvucci (2016), who diagnosed the sign of feedbacks between SSM and next-day precipitation over the United States. They found a similar bimodal spatial structure, with positive feedbacks dominating in the west, and negative feedbacks dominating in the east. Soil moisture memory is a necessary condition for land–atmosphere feedbacks to occur. Short-term memory is the relevant time scale for positive feedbacks between SSM and next-day precipitation. Our results are, therefore, consistent with those of Tuttle and Salvucci (2016). The underestimation of τ_S by the land surface model, relative to satellite observations, suggests that models might fail to reproduce the correct rate of occurrence and intensity of positive SSM–precipitation feedbacks on short time scales.

The land surface model substantially overestimates SSM τ_L in many locations, relative to satellite observations (Fig. 5). A previous study found the Noah land surface model also overestimated τ_L in comparisons with SMAP observations over the continental United States (Shellito et al. 2018). A possible contributing factor to the model overestimation of SSM τ_L is that the land surface model parameters have been overly

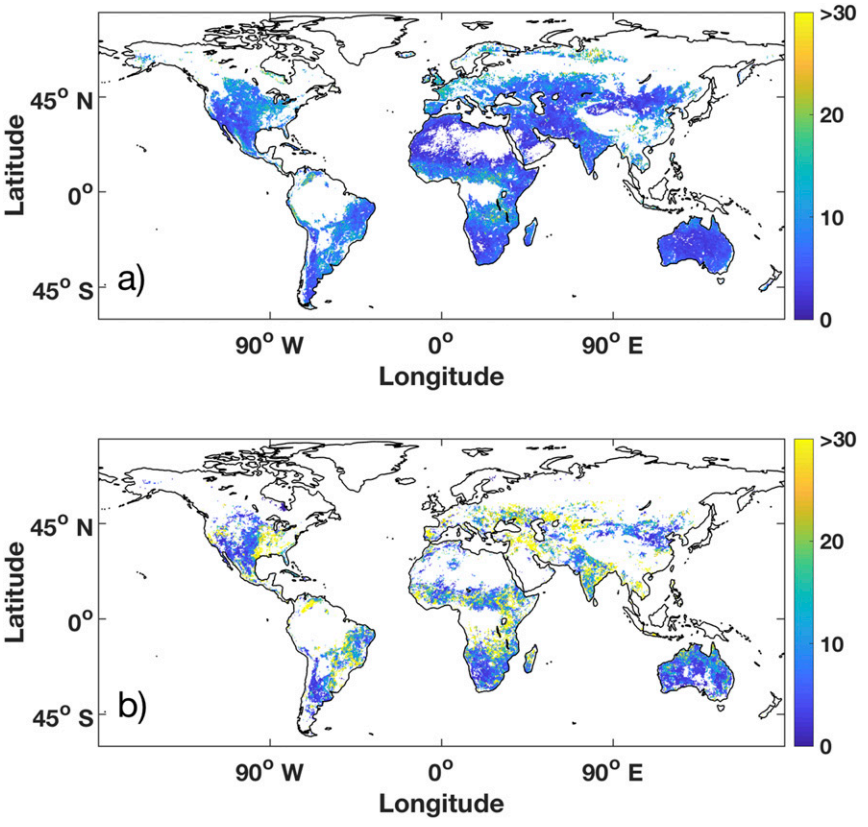

FIG. 5. Global map of median long-term memory τ_L (days) estimated from (a) satellite observations and (b) model SSM.

tuned to point-scale in situ measurements, which dry at a slower rate compared with SMAP observations (Shellito et al. 2016). The drying dynamics at the point scale likely differ considerably from those at the scale of a model grid cell. For example, runoff and subsurface lateral fluxes can play a major role in soil drying at the point scale, but rarely do so at the large scales (~10–100 km) relevant to models and satellites. For instance, in a steep valley, one might expect surface runoff to be a major source of drying at the point scale at higher elevations in the valley. However, if we average over a larger area, that encloses the valley, then the redistribution of water from upslope to downslope has minimal impact on the area-averaged surface soil moisture.

The long-term memory is the relevant time scale for positive feedbacks between SSM and precipitation at weekly, monthly, and seasonal time scales. Sufficient long-term memory is required to sustain feedbacks at these time scales. Therefore, the overestimation of τ_L in the land surface model, relative to satellite observations, suggests that it might overestimate the occurrence rate and intensity of positive SSM–precipitation feedbacks on longer time scales. Over the northern United States, to first order, the opposite bimodal spatial structure is present in satellite observations of τ_L compared to that of τ_S, with τ_L highest in the east and lowest in the west (McColl et al. 2017b). Since the spatial structure is only poorly captured by the model, even after a linear rescaling (Fig. 4a; $R^2 = 0.063$), the model may fail to correctly identify regions where feedbacks occur.

Could ambiguities in the SMAP sensing depth explain the observed differences between SMAP-estimated and model-estimated time scales? While the SMAP sensing depth is nominally 5 cm, in practice it varies with several factors including soil moisture itself. Therefore, the mismatch between model and SMAP estimates could potentially be due to the satellite measuring a deeper soil volume compared to the model, rather than errors in the model. To test this explanation, we compare SMAP-estimated τ_L and τ_S to model RZSM-estimated τ_L (Fig. 6) and τ_S (Fig. 7). If the impact of SMAP measuring deeper than 5 cm is significantly impacting the estimated memory time scales, we would expect a better correspondence between SMAP estimates and model RZSM

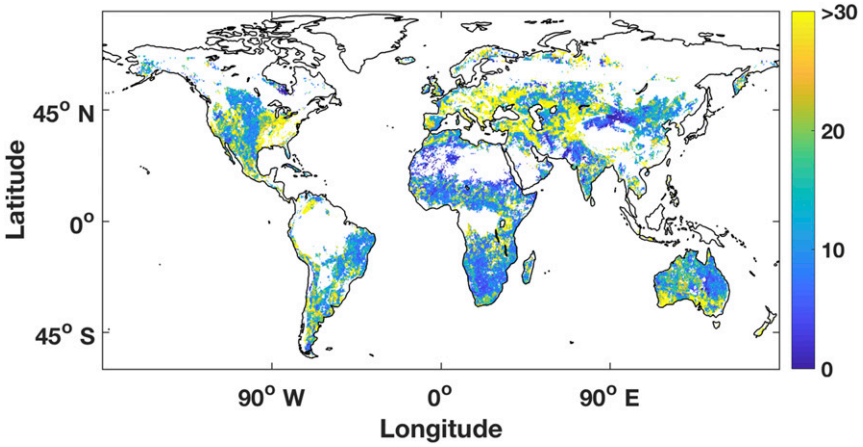

FIG. 6. Global map of median long-term memory τ_L (days) estimated from model RZSM.

estimates, rather than model SSM estimates. However, for both τ_L and τ_S, the model SSM estimate explains more of the observed variance compared to the model RZSM estimate (Fig. 4; 6.3% compared to 3.3% for τ_L, and 51% compared to 0.1% for τ_S). Therefore, differences between the model and satellite do not appear to be dominated by ambiguities in the vertical support of the SMAP observations. It is possible that the SMAP sensing depth is less than 5 cm, or lies between 5 and 100 cm, but we are unable to test these alternatives given the lack of model outputs at these depths.

Modeled soil moisture is known to be highly model dependent (Koster et al. 2009). In particular, the loss function encoded in models can vary substantially (Mahfouf et al. 1996). As such, it is unclear how much one can generalize our comparisons of SMAP estimates with those from one model. However, our comparison is consistent with a recent study (Shellito et al. 2018) that used a different model, which also showed that SSM τ_L is overestimated by the model in most parts of the world, relative to satellite observations.

b. *Joint analysis of τ_L and τ_S*

Globally, short-term and long-term SSM memory are anticorrelated in both the model and satellite observations. Figure 8 shows the joint empirical probability density functions for τ_L and τ_S, estimated using satellite observations and model SSM and RZSM. The Spearman correlation coefficient between τ_L and τ_S globally, using observed SSM, is $\rho = -0.48$ (Fig. 8a); using modeled SSM, it is $\rho = -0.46$ (Fig. 8b). Using modeled RZSM, the anticorrelation disappears ($\rho = 0.051$, Fig. 8c). All three correlations are statistically significant ($p < 0.01$). We use the Spearman correlation coefficient rather than the standard correlation coefficient as the relation between τ_L and τ_S appears nonlinear in all three cases. We conducted sensitivity tests (appendix B) using synthetic soil moisture observations to determine

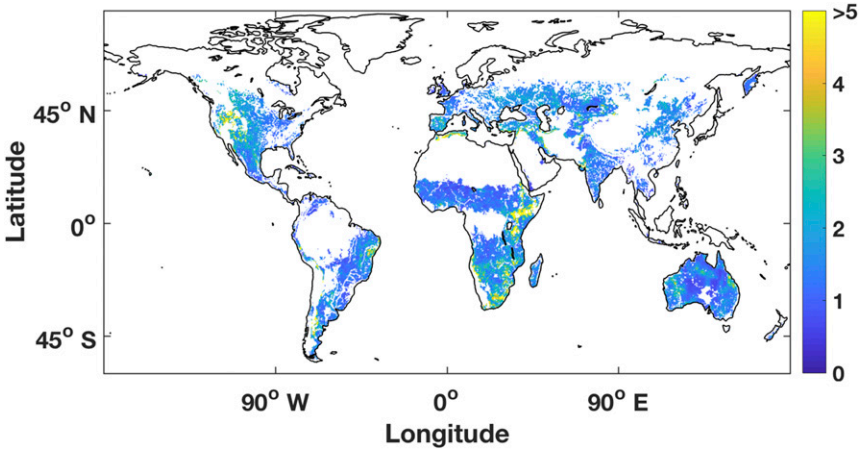

FIG. 7. Global map of short-term memory τ_S (days) estimated from model RZSM.

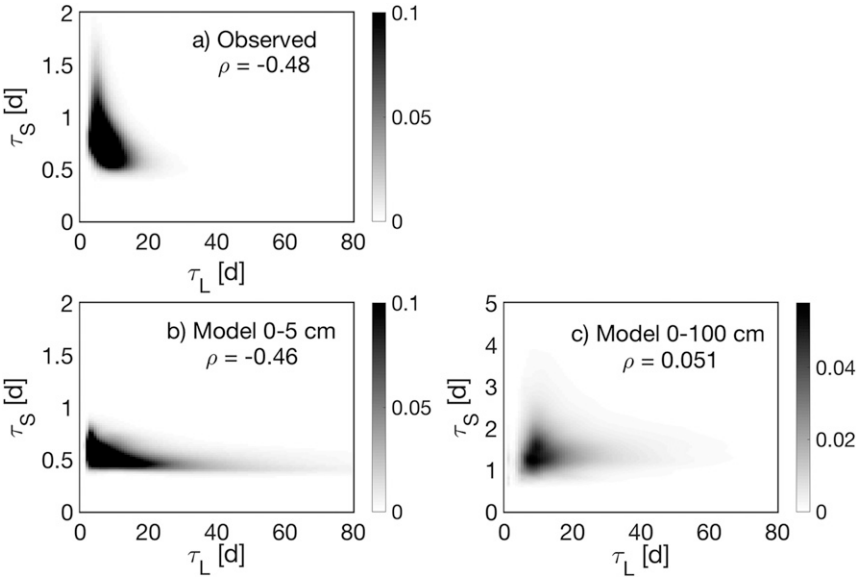

FIG. 8. Joint empirical probability density functions of τ_S and median τ_L, estimated from (a) satellite observations, (b) model SSM, and (c) model RZSM (note the different y-axis scale and colorbar scale in this case).

if the observed anticorrelation could be an artifact of measurement error or violations of assumptions in the estimation procedures for τ_L and τ_S. This could potentially occur if estimation errors in τ_L and τ_S are of opposite sign. Reasonable variations in soil texture, soil moisture observation error and sampling frequency, and climate (including potential evapotranspiration, mean precipitation frequency and intensity, and precipitation seasonality) did not induce substantial biases in τ_L and τ_S of opposite sign (appendix B, Fig. B1). These results suggest the observed anticorrelation between SSM τ_L and τ_S is not an artifact caused by measurement errors or assumptions embedded in the estimation procedure.

Why are τ_S and τ_L spatially anticorrelated? We offer one plausible hypothesis. Consider the effects of a negative spatial anomaly in potential evapotranspiration for an otherwise fixed climate–vegetation–soil system. By definition, this anomaly will increase τ_L (recall that τ_L is inversely proportional to the slope of the loss function in the water-limited stage-II ET regime, and this slope increases with increasing potential evapotranspiration). By reducing evaporative losses, it will also produce a positive surface soil moisture anomaly. Since wetter soils drain more rapidly than drier soils, and drainage is an unresolved process, the anomaly will decrease τ_S. By a similar mechanism, a positive spatial anomaly in potential evapotranspiration will decrease τ_L and increase τ_S. We compared the two memory time scales to relevant biophysical covariates, including soil texture, median soil moisture, and land cover type (not shown). While there was significant unexplained variance in each comparison, median soil moisture explained more variance compared to the other variables tested, consistent with our hypothesis.

The spatial anticorrelation between SSM τ_S and τ_L implies that short-term and long-term land–atmosphere feedbacks will usually occur in different regions. This may partially explain differences in the estimated spatial distribution of land–atmosphere coupling "hot spots" in previous studies (e.g., Koster et al. 2006, 2004; Tuttle and Salvucci 2016), although substantial differences likely also arise due to differences in soil moisture depth, and whether soil moisture observations or model outputs were used. Since standard autocorrelation memory time scales mix τ_S and τ_L, spatial gradients in τ_S and τ_L are smoothed out by autocorrelation memory time scales (appendix C, Figs. C1, C2)

While our sensitivity analysis (appendix B) found that estimates of short- and long-term memory are reasonably robust to uncorrelated noise in the soil moisture observations, it is possible that other forms of observation error could bias their estimation. For example, while estimates of τ_L are robust to additive and multiplicative biases in the observations, estimates of τ_S are only robust to additive biases. Sufficiently large multiplicative biases in the soil moisture time series will lead to overestimation of τ_S. In addition, if errors in the soil moisture time series are autocorrelated, they will lead to overestimation of τ_L. This can occur due to imperfect corrections for vegetation in the soil moisture retrieval algorithm, inducing time-dependent biases that are a function of vegetation

phenology (Dong et al. 2018; Zwieback et al. 2018). We have limited our analysis to annual median values, but future studies on the intra-annual variability of τ_L will need to overcome this limitation in the satellite observations. One possible solution is to use a dual-channel algorithm (e.g., Konings et al. 2016), which retrieves both soil moisture and vegetation optical depth (VOD), rather than a single channel algorithm, which only retrieves soil moisture and requires VOD as an input, which for SMAP is based on an NDVI climatology and subject to substantial errors (Dong et al. 2018).

We have found that annual median SSM short-term and long-term memory time scales are anticorrelated at global scales. However, the short observational record means we are unable to examine temporal variability in memory time scales. This will become possible as the satellite SSM observational record grows with time. Characterizing constraints on SSM–precipitation feedbacks imposed by the seasonal cycle will be a key future research task.

Acknowledgments. Q.H. and H.L. are funded by the National Basic Research Program of China (2015CB953703), the National Key Research and Development Program of China (2017YFA0603703), and the National Natural Science Foundation of China (91537210 and 91747101). K.A.M. acknowledges funding from a Ziff Environmental Fellowship from Harvard University's Center for the Environment. The authors acknowledge funding from the SMAP mission. We thank Andrew Feldman for processing the GPM data. We also thank Paul Dirmeyer and two anonymous reviewers for helpful feedback on an earlier draft of this manuscript.

APPENDIX A

Derivation of Estimator for τ_S

In this appendix, the estimator for τ_S given in Eq. (5) is derived. The hybrid model of soil moisture memory [Eq. (3)] shortly after a precipitation event is

$$\frac{d\theta(t)}{dt} = -\frac{\theta(t) - \overline{\theta}}{\tau_S} + \varepsilon(t), \tag{A1}$$

where $\overline{\theta}$ is mean soil moisture. Taking the expectation of both sides, conditioned on θ, removes the stochastic noise term, resulting in

$$\frac{d\theta(t)}{dt} = -\frac{\theta(t) - \overline{\theta}}{\tau_S} \tag{A2}$$

To solve this ordinary differential equation, we require an initial condition. A precipitation event—marked by a sharp increase in soil moisture—occurs somewhere in the interval $[t - \Delta t, t]$, resulting in a positive increment in the soil moisture time series over the interval $\Delta\theta_+(t) = \theta(t) - \theta(t - \Delta t) > 0$. Define the time of the precipitation event as $t - \Delta t_P$, with Δt_P treated as known for now. Therefore, the initial soil moisture value at the start of the drydown is $\theta(t - \Delta t_P)$. Integrating both sides of Eq. (A2) with respect to t over the interval $[t - \Delta t_P, t]$ and rearranging yields

$$\theta(t) = \overline{\theta} + [\theta(t - \Delta t_P) - \overline{\theta}] \exp\left(-\frac{\Delta t_P}{\tau_S}\right). \tag{A3}$$

Taking the mean of Eq. (A3), conditioned on Δt_P, and applying assumptions R2 and R3 results in

$$\overline{\theta}(t|\Delta t_P) = \overline{\theta(t - \Delta t)} + \frac{\alpha}{\Delta z} \exp\left(-\frac{\Delta t_P}{\tau_S}\right). \tag{A4}$$

Since, in practice, we do not know Δt_P, it is treated as a random variable. To eliminate the conditional dependence on Δt_P, we apply assumption R1:

$$\overline{\theta}(t) = \int_{-\infty}^{\infty} \overline{\theta}(t|\Delta t_P) f_{\Delta T_P}(\Delta t_P)\, d\Delta t_P = \overline{\theta(t - \Delta t)} + \frac{\alpha}{\Delta z}\frac{\tau_S}{\Delta t}\left[1 - \exp\left(-\frac{\Delta t}{\tau_S}\right)\right], \tag{A5}$$

where

$$f_{\Delta T_P}(\Delta t_P) = \begin{cases} \dfrac{1}{\Delta t}, & \text{for } 0 \le \Delta t_P \le \Delta t, \\ 0, & \text{otherwise}. \end{cases} \tag{A6}$$

Applying the Taylor expansion $\exp(x) \approx 1 + x + x^2/2 + \cdots$ to the exponential term on the right-hand side, and limiting terms to first order, results in the first-order approximation

$$\overline{\theta}(t) \approx \overline{\theta(t - \Delta t)} + \frac{\alpha}{\Delta z} \exp\left(-\frac{\Delta t}{2\tau_S}\right). \tag{A7}$$

Rearranging gives

$$\tau_S = -\frac{\frac{\Delta t}{2}}{\log\left(\frac{\Delta z \overline{\Delta\theta_+}}{\alpha}\right)}. \tag{A8}$$

APPENDIX B

Sensitivity Experiments with Synthetic Data

We test our estimation procedures for τ_S and τ_L, and their embedded assumptions, on synthetic soil moisture

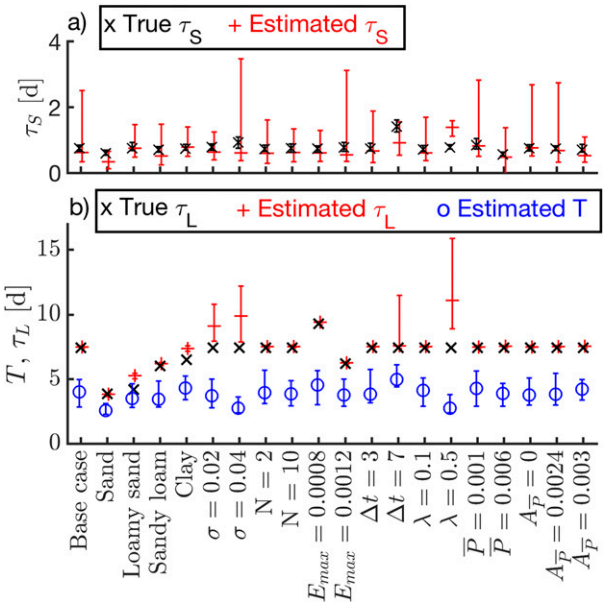

FIG. B1. Sensitivity analysis of estimated time scales (a) τ_S and (b) median τ_L, and T, based on synthetic soil moisture time series, for which the true value is known. The synthetic soil moisture time series were generated using a model with prescribed loss function, and forced with stochastic precipitation. Parameters are defined in Tables B1 and B2. For each set of parameters used in the sensitivity analysis, we ran the stochastic model 30 times, generating 30 replicates of τ_S, τ_L, and T, which were used to estimate 90% confidence intervals.

TABLE B1. Default parameters used in the synthetic model sensitivity study.

Parameter	Default value
Soil texture	Loam
Potential evapotranspiration $E_{\max}$	1×10^{-3} m day^{-1}
Sample size N	2 years
Sampling frequency $1/\Delta t$	1/3 day^{-1}
Standard deviation of observation noise error σ	0
Mean daily precipitation $\overline{P}$	3×10^{-3} m day^{-1}
Mean precipitation event interarrival time $1/\lambda$	3 days
Amplitude of seasonal cycle of mean daily precipitation $A_{\overline{P}}$	3×10^{-3} m day^{-1}

"observations," generated using a stochastic model of soil moisture. The model is similar to that presented in Laio et al. (2001) and its key features are described here. Precipitation event interarrival times are modeled as independent exponential random variables with mean $1/\lambda$. The total precipitation for a given event is also modeled as an exponential random variable with mean α. The mean daily precipitation, therefore, is $\overline{P} = \alpha\lambda$. In addition, unlike Laio et al. (2001), we include a seasonal cycle in precipitation represented as

$$\overline{P}(t) = \overline{P_0} + A_{\overline{P}} \sin\left(\frac{2\pi t}{12}\right) \tag{B1}$$

similar to the form used in Feng et al. (2014), where t is the month, $\overline{P_0}$ is the annually averaged mean daily precipitation, and $A_{\overline{P}}$ is the amplitude of the seasonal cycle. For fixed λ, this gives an implicit seasonal cycle in α.

Losses from the soil column L comprise ET and vertical drainage. Runoff—defined here as horizontal transport of water over or through the SSM control volume—is assumed to be negligible at the large horizontal scales relevant to a satellite footprint or a model grid cell. Note that runoff excludes baseflow since the SSM control volume, with a depth of ~5 cm, rarely intersects the water table. The combined losses are represented by a loss function similar to that given in Fig. 1. It includes a linear, stage-II ET regime $\{L = [(s - s_w)/(s_* - s_w)]E_{\max}$, where $s = \theta/n$ is soil saturation, n is soil porosity, s_w is the wilting point, and s_* is a critical soil saturation at which the transition from stage-I to stage-II ET occurs$\}$; a flat, stage-I ET regime ($L = E_{\max}$); and a drainage regime represented by a power law

$$L = \frac{K_s\{\exp[\beta(s - s_{\text{fc}})] - 1\}}{\exp[\beta(1 - s_{\text{fc}})] - 1},$$

where s_{fc} is field capacity, K_s is the saturated hydraulic conductivity, and β is a parameter used to fit the expression to data.

The model is integrated at a 1-min time step. When precipitation falls, it falls entirely within a 1-min time step, a simplification that is unrealistic but sufficient for the purposes of this sensitivity analysis. For each set of parameters used in the sensitivity analysis, we run the stochastic model 30 times, generating 30 replicates of τ_S, τ_L, and T, which are used to estimate 90% confidence intervals in Fig. B1. Parameters are defined in Tables B1 and B2.

The autocorrelation time scale T is obtained from the estimated autocorrelation function of the time series, corresponding to the time lag at which the autocorrelation function equals e^{-1}. Since T is very significantly biased by seasonality, we remove the monthly soil moisture climatology (estimated from the available synthetic observations for the given sensitivity experiment) before estimating T. The results do not change qualitatively if a 30-day moving window average is subtracted instead. We do not remove the seasonal cycle when estimating τ_S and τ_L, since they are designed to be insensitive to the seasonal cycle (a significant advantage over T).

TABLE B2. Soil texture parameters used in synthetic sensitivity study, based on Laio et al. (2001).

Soil texture	Saturated hydraulic conductivity K_s (m day^{-1})	Porosity n	Drainage loss parameter β	Wilting point s_w	Critical soil saturation s_*	Field capacity s_{fc}
Sand	2	0.35	12.1	0.11	0.33	0.35
Loamy sand	1	0.42	12.7	0.11	0.31	0.52
Sandy loam	0.8	0.43	13.8	0.18	0.46	0.56
Loam	0.2	0.45	14.8	0.24	0.57	0.65
Clay	0.1	0.5	26.8	0.52	0.78	0.99

The e-folding autocorrelation time scale T consistently underestimates the true long-term memory (Fig. B1). This is due to detrending: in an attempt to remove seasonality from the soil moisture time series (which would otherwise dominate the estimate of T and cause it to be substantially positively biased), the time series is overcorrected. Some variability relevant to the short-term memory is removed, resulting in the underestimate. This problem is fundamentally due to the inapplicability of the red noise model at submonthly time scales.

Estimates of τ_L and τ_S are reasonable for a variety of loss functions (corresponding to variations in soil texture and $E_{\max}$), sample sizes N and precipitation regimes (varying λ, $\overline{P}$, and A_P), although τ_L is overestimated for high λ. In this case, precipitation occurs frequently but at low intensity. These climates do not typically support major soil moisture–precipitation feedbacks, because the precipitation variability signal is too low. These regions are automatically filtered out of our analyses by excluding regions where very few drydowns are identified.

Errors in soil moisture observations can bias or reduce the precision of estimates of τ_S and τ_L. Figure B1 shows the sensitivity of estimates of τ_S and τ_L to observation error. Here, observation errors are assumed to be additive, Gaussian and independent in time. The standard deviation of the error term is varied between zero (base case), 0.02, and 0.04. The highest error case corresponds to an extreme case in which the nominal estimated

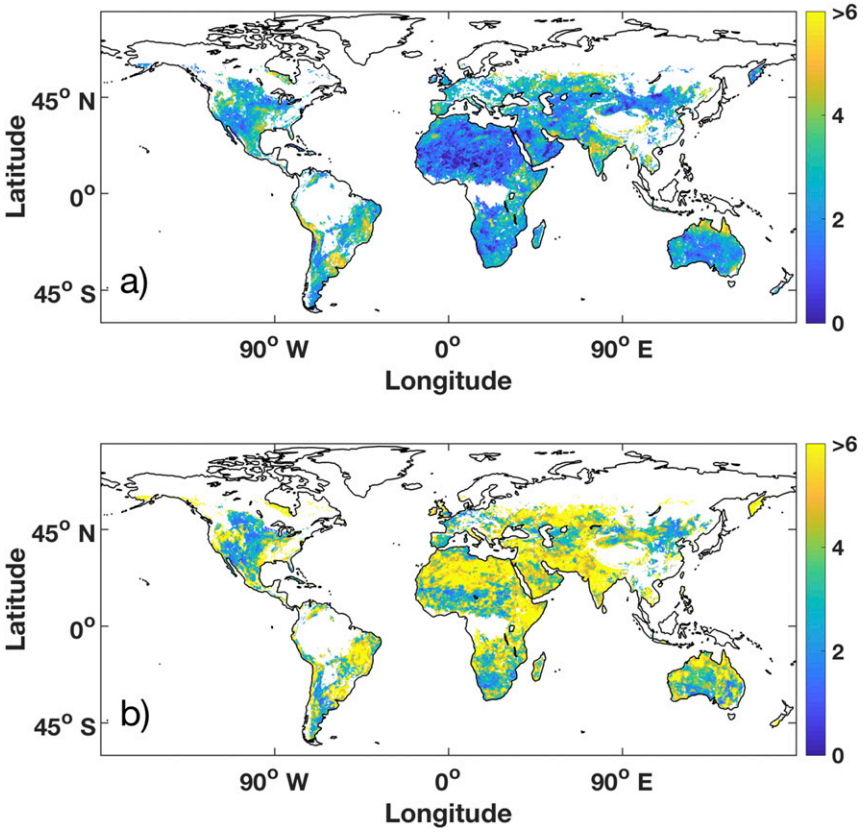

FIG. C1. Global map of T (days) estimated from (a) satellite observations and (b) model SSM.

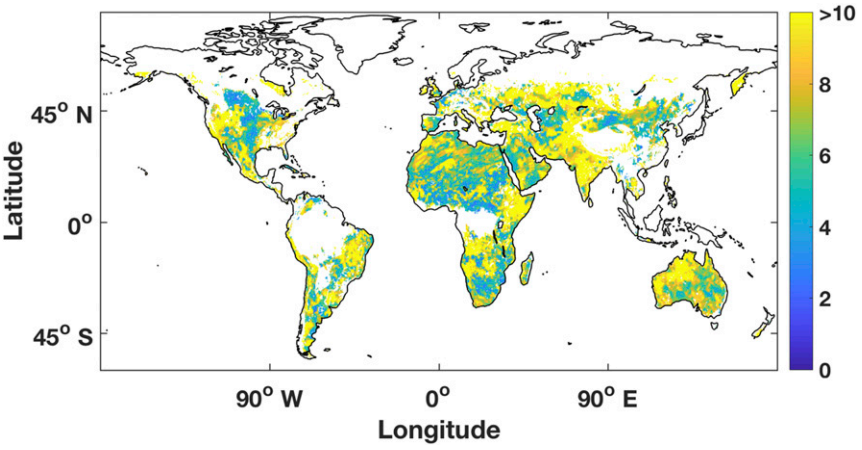

FIG. C2. Global map of T (days) estimated from model RZSM.

SMAP observation error is contributed entirely by noise, with no contribution from biases. The addition of observation noise decreases the precision of estimates of both τ_S and τ_L, particularly for τ_L. It also introduces positive biases into estimates of both τ_S and τ_L. McColl et al. (2017a) provide an error analysis showing that F_P is positively biased in the presence of noise, consistent with these results. However, the biases in τ_S and τ_L are relatively small. Even in the most extreme case (Fig. B1, $\sigma = 0.04$), the median estimated τ_L is closer to the true value than T, which decreases with increasing observation error.

The sampling frequency of the observations impacts estimates of τ_S and τ_L. As the sampling frequency decreases (i.e., Δt gets larger), the parameterized time scale τ_S gets longer. For small Δt, only drainage losses are parameterized; since these losses are relatively rapid, τ_S is relatively small. For larger Δt, a combination of drainage losses and ET losses are parameterized; since ET losses are relatively slower, τ_S is relatively larger in this case. Estimates of τ_S are reasonable at relatively high sampling frequencies, including the SMAP sampling frequency ($\Delta t = 3$ days). Long-term memory τ_L does not vary with sampling frequency, since it is resolved by the observations in all cases, rather than parameterized. T systematically underestimates the long-term memory, and increases slightly with increasing Δt. On the other hand, estimates of τ_L agree reasonably with the true value, particularly for the default case corresponding to the SMAP sampling frequency ($\Delta t = 3$ days).

APPENDIX C

Mixing of Memory Time Scales by Traditional Memory Metrics

Figures C1 and C2 show the e-folding autocorrelation time scale T, estimated using satellite observations, and model SSM and RZSM. Comparison of Fig. C1 with Figs. 3 and 5 (which show equivalent maps of SSM τ_S and τ_L, respectively) reveals that, in most parts of the world, values of T are typically less than τ_L and greater than τ_S. This is also true for model RZSM T (cf. Fig. C2 with Figs. 6 and 7). These results are consistent with the idea that T mixes the two distinct time scales τ_L and τ_S in both the model and the observations.

REFERENCES

Akbar, R., D. J. Short Gianotti, K. A. McColl, E. Haghighi, G. D. Salvucci, and D. Entekhabi, 2018a: Estimation of landscape soil water losses from satellite observations of soil moisture. *J. Hydrometeor.*, **19**, 871–889, https://doi.org/10.1175/JHM-D-17-0200.1.

——, ——, ——, ——, ——, and ——,2018b: Hydrological storage length scales represented by remote sensing estimates of soil moisture and precipitation. *Water Resour. Res.*, **54**, 1476–1492, https://doi.org/10.1002/2017WR021508.

Chan, S. K., and Coauthors, 2016: Assessment of the SMAP Passive Soil Moisture Product. *IEEE Trans. Geosci. Remote Sens.*, **54**, 4994–5007, https://doi.org/10.1109/TGRS.2016.2561938.

Chen, F., W. T. Crow, R. Bindlish, A. Colliander, M. S. Burgin, J. Asanuma, and K. Aida, 2018: Global-scale evaluation of SMAP, SMOS and ASCAT soil moisture products using triple collocation. *Remote Sens. Environ.*, **214**, 1–13, https://doi.org/10.1016/j.rse.2018.05.008.

Colliander, A., and Coauthors, 2017: Validation of SMAP surface soil moisture products with core validation sites. *Remote Sens. Environ.*, **191**, 215–231, https://doi.org/10.1016/j.rse.2017.01.021.

Delworth, T. L., and S. Manabe, 1988: The influence of potential evaporation on the variabilities of simulated soil wetness and climate. *J. Climate*, **1**, 523–547, https://doi.org/10.1175/1520-0442(1988)001<0523:TIOPEO>2.0.CO;2.

——, and ——, 1989: The influence of soil wetness on near-surface atmospheric variability. *J. Climate*, **2**, 1447–1462, https://doi.org/10.1175/1520-0442(1989)002<1447:TIOSWO>2.0.CO;2.

Dirmeyer, P. A., and H. E. Norton, 2018: Indications of surface and sub-surface hydrologic properties from SMAP soil moisture retrievals. *Hydrology*, **5**, 36, https://doi.org/10.3390/hydrology5030036.

——, and Coauthors, 2016: Confronting weather and climate models with observational data from soil moisture networks over the United States. *J. Hydrometeor.*, **17**, 1049–1067, https://doi.org/10.1175/JHM-D-15-0196.1.

Dong, J., W. T. Crow, and R. Bindlish, 2018: The error structure of the SMAP single and dual channel soil moisture retrievals. *Geophys. Res. Lett.*, **45**, 758–765, https://doi.org/10.1002/2017GL075656.

Ducharne, A., R. D. Koster, M. J. Suarez, M. Stieglitz, and P. Kumar, 2000: A catchment-based approach to modeling land surface processes in a general circulation model: 2. Parameter estimation and model demonstration. *J. Geophys. Res.*, **105**, 24 823–24 838, https://doi.org/10.1029/2000JD900328.

Entekhabi, D., and Coauthors, 2010: The Soil Moisture Active Passive (SMAP). *Mission. Proc. IEEE*, **98**, 704–716, https://doi.org/10.1109/JPROC.2010.2043918.

Entin, J. K., A. Robock, K. Y. Vinnikov, S. E. Hollinger, S. Liu, and A. Namkhai, 2000: Temporal and spatial scales of observed soil moisture variations in the extratropics. *J. Geophys. Res.*, **105**, 11 865–11 877, https://doi.org/10.1029/2000JD900051.

Feng, X., A. Porporato, and I. Rodriguez-Iturbe, 2014: Stochastic soil water balance under seasonal climates. *Proc. Roy. Soc. London*, **A471**, 20140623, https://doi.org/10.1098/rspa.2014.0623.

Findell, K. L., and E. A. B. Eltahir, 2003a: Atmospheric controls on soil moisture–boundary layer interactions. Part I: Framework development. *J. Hydrometeor.*, **4**, 552–569, https://doi.org/10.1175/1525-7541(2003)004<0552:ACOSML>2.0.CO;2.

——, and ——, 2003b: Atmospheric controls on soil moisture–boundary layer interactions. Part II: Feedbacks within the continental United States. *J. Hydrometeor.*, **4**, 570–583, https://doi.org/10.1175/1525-7541(2003)004<0570:ACOSML>2.0.CO;2.

Ford, T. W., E. Harris, and S. M. Quiring, 2014: Estimating root zone soil moisture using near-surface observations from SMOS. *Hydrol. Earth Syst. Sci.*, **18**, 139–154, https://doi.org/10.5194/hess-18-139-2014.

Gentine, P., A. A. M. Holtslag, F. D'Andrea, and M. Ek, 2013: Surface and atmospheric controls on the onset of moist convection over land. *J. Hydrometeor.*, **14**, 1443–1462, https://doi.org/10.1175/JHM-D-12-0137.1.

Ghannam, K., T. Nakai, A. Paschalis, C. A. Oishi, A. Kotani, Y. Igarashi, T. Kumagai, and G. G. Katul, 2016: Persistence and memory timescales in root-zone soil moisture dynamics. *Water Resour. Res.*, **52**, 1427–1445, https://doi.org/10.1002/2015WR017983.

Guillod, B. P., B. Orlowsky, D. G. Miralles, A. J. Teuling, and S. I. Seneviratne, 2015: Reconciling spatial and temporal soil moisture effects on afternoon rainfall. *Nat. Commun.*, **6**, 6443, https://doi.org/10.1038/ncomms7443.

Honnert, R., 2016: Representation of the grey zone of turbulence in the atmospheric boundary layer. *Adv. Sci. Res.*, **13**, 63–67, https://doi.org/10.5194/asr-13-63-2016.

Huffman, G., 2017: GPM_3IMERGHH: GPM IMERG Final Precipitation L3 Half Hourly 0.1 degree × 0.1 degree V05. Goddard Earth Sciences Data and Information Services Center (GES DISC), accessed 13 May 2019, https://doi.org/10.5067/GPM/IMERG/3B-HH/05.

Katul, G. G., A. Porporato, E. Daly, A. C. Oishi, H.-S. Kim, P. C. Stoy, J.-Y. Juang, and M. B. Siqueira, 2007: On the spectrum of soil moisture from hourly to interannual scales. *Water Resour. Res.*, **43**, https://doi.org/10.1029/2006WR005356.

Klein, S. A., X. Jiang, J. Boyle, S. Malyshev, and S. Xie, 2006: Diagnosis of the summertime warm and dry bias over the U.S. Southern Great Plains in the GFDL climate model using a weather forecasting approach. *Geophys. Res. Lett.*, **33**, L18805, https://doi.org/10.1029/2006GL027567.

Konings, A. G., M. Piles, K. Rötzer, K. A. McColl, S. K. Chan, and D. Entekhabi, 2016: Vegetation optical depth and scattering albedo retrieval using time series of dual-polarized L-band radiometer observations. *Remote Sens. Environ.*, **172**, 178–189, https://doi.org/10.1016/j.rse.2015.11.009.

Koster, R. D., 2015: ''Efficiency space'': A framework for evaluating joint evaporation and runoff behavior. *Bull. Amer. Meteor. Soc.*, **96**, 393–396, https://doi.org/10.1175/BAMS-D-14-00056.1.

——, and S. P. P. Mahanama, 2012: Land surface controls on hydroclimatic means and variability. *J. Hydrometeor.*, **13**, 1604–1620, https://doi.org/10.1175/JHM-D-12-050.1.

——, and P. C. D. Milly, 1997: The interplay between transpiration and runoff formulations in land surface schemes used with atmospheric models. *J. Climate*, **10**, 1578–1591, https://doi.org/10.1175/1520-0442(1997)010<1578:TIBTAR>2.0.CO;2.

——, and M. J. Suarez, 2001: Soil moisture memory in climate models. *J. Hydrometeor.*, **2**, 558–570, https://doi.org/10.1175/1525-7541(2001)002<0558:SMMICM>2.0.CO;2.

——, ——, A. Ducharne, M. Stieglitz, and P. Kumar, 2000: A catchment-based approach to modeling land surface processes in a general circulation model: 1. Model structure. *J. Geophys. Res.*, **105**, 24 809–24 822, https://doi.org/10.1029/2000JD900327.

——, and Coauthors, 2004: Regions of strong coupling between soil moisture and precipitation. *Science*, **305**, 1138–1140, https://doi.org/10.1126/science.1100217.

——, and Coauthors, 2006: GLACE: The Global Land–Atmosphere Coupling Experiment. Part I: Overview. *J. Hydrometeor.*, **7**, 590–610, https://doi.org/10.1175/JHM510.1.

——, Z. Guo, R. Yang, P. A. Dirmeyer, K. Mitchell, and M. J. Puma, 2009: On the nature of soil moisture in land surface models. *J. Climate*, **22**, 4322–4335, https://doi.org/10.1175/2009JCLI2832.1.

——, R. H. Reichle, and S. P. P. Mahanama, 2017: A data-driven approach for daily real-time estimates and forecasts of near-surface soil moisture. *J. Hydrometeor.*, **18**, 837–843, https://doi.org/10.1175/JHM-D-16-0285.1.

Laio, F., A. Porporato, L. Ridolfi, and I. Rodriguez-Iturbe, 2001: Plants in water-controlled ecosystems: active role in hydrologic processes and response to water stress: II. Probabilistic soil moisture dynamics. *Adv. Water Resour.*, **24**, 707–723, https://doi.org/10.1016/S0309-1708(01)00005-7.

Ma, H.-Y., and Coauthors, 2014: On the correspondence between mean forecast errors and climate errors in CMIP5 models. *J. Climate*, **27**, 1781–1798, https://doi.org/10.1175/JCLI-D-13-00474.1.

——, and Coauthors, 2018: CAUSES: On the role of surface energy budget errors to the warm surface air temperature error over the central United States. *J. Geophys. Res. Atmos.*, **123**, 2888–2909, https://doi.org/10.1002/2017JD027194.

Mahfouf, J.-F., and Coauthors, 1996: Analysis of transpiration results from the RICE and PILPS workshop. *Global Planet. Change*, **13**, 73–88, https://doi.org/10.1016/0921-8181(95)00039-9.

McColl, K. A., S. H. Alemohammad, R. Akbar, A. G. Konings, S. Yueh, and D. Entekhabi, 2017a: The global distribution and dynamics of surface soil moisture. *Nat. Geosci.*, **10**, 100, https://doi.org/10.1038/ngeo2868.

——, W. Wang, B. Peng, R. Akbar,D. J. Short Gianotti, H. Lu, M. Pan, and D. Entekhabi, 2017b: Global characterization of surface soil moisture drydowns. *Geophys. Res. Lett.*, **44**, 3682–3690, https://doi.org/10.1002/2017GL072819.

Miralles, D. G., A. J. Teuling, C. C. van Heerwaarden, and J. Vilà-Guerau de Arellano, 2014: Mega-heatwave temperatures due to combined soil desiccation and atmospheric heat accumulation. *Nat. Geosci.*, **7**, 345–349, https://doi.org/10.1038/ngeo2141.

Morcrette, C. J., and Coauthors, 2018: Introduction to CAUSES: Description of weather and climate models and their near-surface temperature errors in 5 day hindcasts near the Southern Great Plains. *J. Geophys. Res. Atmos.*, **123**, 2655–2683, https://doi.org/10.1002/2017JD027199.

Nakai, T., G. G. Katul, A. Kotani, Y. Igarashi, T. Ohta, M. Suzuki, and T. Kumagai, 2014: Radiative and precipitation controls on root zone soil moisture spectra. *Geophys. Res. Lett.*, **41**, 7546–7554, https://doi.org/10.1002/2014GL061745.

O'Neill, P. E., S. Chan, E. G. Njoku, T. Jackson, and R. Bindlish, 2018: SMAP L3 Radiometer Global Daily 36 km EASE-Grid Soil Moisture, Version 4. National Snow and Ice Data Center Distributed Active Archive Center, accessed 4 April 2017, https://doi.org/10.5067/ZX7YX2Y2LHEB.

Reichle, R. H., and Coauthors, 2017a: Assessment of the SMAP Level-4 surface and root-zone soil moisture product using in situ measurements. *J. Hydrometeor.*, **18**, 2621–2645, https://doi.org/10.1175/JHM-D-17-0063.1.

——, Q. Liu, R. D. Koster, C. S. Draper, S. P. P. Mahanama, and G. S. Partyka, 2017b: Land surface precipitation in MERRA-2. *J. Climate*, **30**, 1643–1664, https://doi.org/10.1175/JCLI-D-16-0570.1.

Rondinelli, W. J., B. K. Hornbuckle, J. C. Patton, M. H. Cosh, V. A. Walker, B. D. Carr, and S. D. Logsdon, 2015: Different rates of soil drying after rainfall are observed by the SMOS satellite and the South Fork in situ Soil Moisture Network. *J. Hydrometeor.*, **16**, 889–903, https://doi.org/10.1175/JHM-D-14-0137.1.

Roundy, J. K., C. R. Ferguson, and E. F. Wood, 2013: Temporal variability of land–atmosphere coupling and its implications for drought over the southeast United States. *J. Hydrometeor.*, **14**, 622–635, https://doi.org/10.1175/JHM-D-12-090.1.

——, ——, and ——, 2014: Impact of land-atmospheric coupling in CFSv2 on drought prediction. *Climate Dyn.*, **43**, 421–434, https://doi.org/10.1007/s00382-013-1982-7.

Saleem, J. A., and G. D. Salvucci, 2002: Comparison of soil wetness indices for inducing functional similarity of hydrologic response across sites in Illinois. *J. Hydrometeor.*, **3**, 80–91, https://doi.org/10.1175/1525-7541(2002)003<0080:COSWIF>2.0.CO;2.

Salvucci, G. D., 2001: Estimating the moisture dependence of root zone water loss using conditionally averaged precipitation. *Water Resour. Res.*, **37**, 1357–1365, https://doi.org/10.1029/2000WR900336.

Santanello, J. A., and Coauthors, 2018: Land–atmosphere interactions: The LoCo perspective. *Bull. Amer. Meteor. Soc.*, **99**, 1253–1272, https://doi.org/10.1175/BAMS-D-17-0001.1.

Seneviratne, S. I., and R. D. Koster, 2012: A revised framework for analyzing soil moisture memory in climate data: Derivation and interpretation. *J. Hydrometeor.*, **13**, 404–412, https://doi.org/10.1175/JHM-D-11-044.1.

——, and Coauthors, 2006: Soil moisture memory in AGCM simulations: Analysis of Global Land–Atmosphere Coupling Experiment (GLACE) data. *J. Hydrometeor.*, **7**, 1090–1112, https://doi.org/10.1175/JHM533.1.

——, T. Corti, E. L. Davin, M. Hirschi, E. B. Jaeger, I. Lehner, B. Orlowsky, and A. J. Teuling, 2010: Investigating soil moisture–climate interactions in a changing climate: A review. *Earth-Sci. Rev.*, **99**, 125–161, https://doi.org/10.1016/j.earscirev.2010.02.004.

Shellito, P. J., and Coauthors, 2016: SMAP soil moisture drying more rapid than observed in situ following rainfall events. *Geophys. Res. Lett.*, **43**, 8068– 8075, https://doi.org/10.1002/2016GL069946.

——, E. E. Small, and B. Livneh, 2018: Controls on surface soil drying rates observed by SMAP and simulated by the Noah land surface model. *Hydrol. Earth Syst. Sci.*, **22**, 1649–1663, https://doi.org/10.5194/hess-22-1649-2018.

Tuttle, S. E., and G. D. Salvucci, 2014: A new approach for validating satellite estimates of soil moisture using large-scale precipitation: Comparing AMSR-E products. *Remote Sens. Environ.*, **142**, 207–222, https://doi.org/10.1016/j.rse.2013.12.002.

——, and ——, 2016: Empirical evidence of contrasting soil moisture–precipitation feedbacks across the United States. *Science*, **352**, 825–828, https://doi.org/10.1126/science.aaa7185.

Vinnikov, K. Y., and I. B. Yeserkepova, 1991: Soil moisture: Empirical data and model results. *J. Climate*, **4**, 66–79, https://doi.org/10.1175/1520-0442(1991)004<0066:SMEDAM>2.0.CO;2.

Wyngaard, J. C., 2004: Toward numerical modeling in the "terra incognita." *J. Atmos. Sci.*, **61**, 1816–1826, https://doi.org/10.1175/1520-0469(2004)061<1816:TNMITT>2.0.CO;2.

Zwieback, S., A. Colliander, M. H. Cosh, J. Martínez-Fernández, H. McNairn, P. J. Starks, M. Thibeault, and A. Berg, 2018: Estimating time-dependent vegetation biases in the SMAP soil moisture product. *Hydrol. Earth Syst. Sci.*, **22**, 4473–4489, https://doi.org/10.5194/hess-22-4473-2018.